

Acoustic Predictions of Manned and Unmanned Rotorcraft Using the Comprehensive Analytical Rotorcraft Model for Acoustics (CARMA) Code System

D. Douglas Boyd, Jr.
Aero and Structural Acoustics Branch
NASA Langley Research Center
Hampton, VA 23681-2199

Casey L. Burley
Aero and Structural Acoustics Branch
NASA Langley Research Center
Hampton, VA 23681-2199

David A. Conner
U.S. Army RDECOM, AMRDEC
AeroFlightDynamics Directorate, Joint Research Program Office
Langley Research Center
Hampton, VA 23681-2199

American Helicopter Society International Specialists' Meeting on Unmanned Rotorcraft
January 18-20, 2005, Phoenix, Arizona, USA

Abstract

The Comprehensive Analytical Rotorcraft Model for Acoustics (CARMA) is being developed under the Quiet Aircraft Technology Project within the NASA Vehicle Systems Program. The purpose of CARMA is to provide analysis tools for the design and evaluation of efficient low-noise rotorcraft, as well as support the development of safe, low-noise flight operations. The baseline prediction system of CARMA is presented and current capabilities are illustrated for a model rotor in a wind tunnel, a rotorcraft in flight and for a notional coaxial rotor configuration; however, a complete validation of the CARMA system capabilities with respect to a variety of measured databases is beyond the scope of this work. For the model rotor illustration, predicted rotor airloads and acoustics for a BO-105 model rotor are compared to test data from HART-II. For the flight illustration, acoustic data from an MD-520N helicopter flight test, which was conducted at Eglin Air Force Base in September 2003, are compared with CARMA full vehicle flight predictions. Predicted acoustic metrics at three microphone locations are compared for limited level flight and descent conditions. Initial acoustic predictions using CARMA for a notional coaxial rotor system are made. The effect of increasing the vertical separation between the rotors on the predicted airloads and acoustic results are shown for both aerodynamically non-interacting and aerodynamically interacting rotors. The sensitivity of including the aerodynamic interaction effects of each rotor on the other, especially when the rotors are in close proximity to one another is initially examined. The predicted coaxial rotor noise is compared to that of a conventional single rotor system of equal thrust, where both are of reasonable size for an unmanned aerial vehicle (UAV).

Introduction

A number of techniques may be employed to determine acoustic footprints of rotorcraft vehicles. One method is to directly measure the acoustic footprint during a wind tunnel or flight test. For example, in a series of flight tests on the XV-15 tilt-rotor aircraft, the acoustic footprint was measured for various flight conditions and flight paths [ref. 1, 2]. These flight tests were used to develop low-noise flight procedures and to assess their impact on the ground noise footprint. Another example of a flight test is the "Acoustic Week Flight Test" conducted at Eglin Air Force Base in September 2003 [ref. 3]. This flight test measured acoustic data for a number of rotorcraft vehicles operating in level flight over a range of airspeeds. Manned and unmanned aerial

vehicles (UAV) were tested including a Bell-206, an AH-64A, a K-MAX, a 4-bladed developmental prototype UAV based on the Schweizer Model 269D helicopter, an Aerostar UAV, a BO-105, a UH-60L, and an MD-520N. Acoustic footprints have also been measured in wind tunnel tests. For example, the first Higher-harmonic-control Aeroacoustic Rotor Test (HART-I) [ref. 4] and the HART-II [ref. 5] wind tunnel tests mapped the noise footprints of a 40% dynamically scaled BO-105 model rotor for both non-HHC (Higher Harmonic Control) and HHC conditions. The main objective of those tests has been to improve the basic understanding and analytical modeling capabilities for rotor blade-vortex interaction noise with and without HHC inputs. Flight and wind tunnel tests such as these are valuable, but can be cost prohibitive, especially if numerous vehicles, configurations, flight conditions, and/or wind tunnel conditions are to be explored.

Prediction methods can also be used to estimate rotorcraft acoustic footprints. These types of methods have been under development for many years. For example, the Tilt-Rotor Aeroacoustics Code (TRAC) [ref. 6, 7, 8, 9] was developed in the mid- to late-1990s as a rotorcraft noise prediction system with emphasis on computing acoustics for tilt-rotors. This successful effort was not only demonstrated for model and full-scale tilt-rotors but conventional rotorcraft designs as well. The TRAC prediction system architecture philosophy and capabilities are being adapted for use in the development of the current “Comprehensive Analytical Rotorcraft Model for Acoustics,” or CARMA system. CARMA utilizes a newer, more general comprehensive rotorcraft aeromechanics code than that used in TRAC. Also, newer acoustic source noise analyses and propagation codes that have been developed since TRAC are being used.

In this paper, the baseline CARMA prediction system is presented and its current capabilities are illustrated with prediction examples for a model rotor in a wind tunnel, a rotorcraft in flight and for a notional coaxial rotor configuration. For the model rotor illustration, predicted rotor airloads and acoustics for a BO-105 model rotor are computed and the results are compared to test data from HART-II for the non-HHC baseline condition. For the flight illustration, acoustic data from an MD-520N helicopter flight test are compared with CARMA full vehicle flight predictions. The prediction model accounts for the main rotor and the NOTAR tail force and thus illustrates the CARMA capabilities for the full vehicle trim in realistic flight conditions. Acoustic metric time histories predicted at three of the measurement microphone locations for a level flight and a mild descent condition are presented and compared with the measured results. A notional coaxial rotor system is constructed using two BO-105 model rotors, which are separated vertically on the same rotor shaft axis. Example predictions of the rotor airloads and acoustics are shown for both aerodynamically non-interacting and aerodynamically interacting rotors with different separation distances. The sensitivity of including the aerodynamic interaction effects of each rotor on the other, especially when the rotors are in close proximity to one another is initially examined. Since this work is built on a model scale rotor, it is directly applicable to, and is the approximate size of, several unmanned coaxial-type vehicle configurations such as the Sentinel series of vehicles [ref. 10]. Finally, the noise for this notional coaxial rotor system is predicted for the same thrust condition as the conventional single main rotor system and the acoustic results are compared.

Acoustic Prediction Method: CARMA

The rotorcraft noise prediction system CARMA is being developed under the Quiet Aircraft Technology Project within the NASA Vehicle Systems Program. The purpose of CARMA is to provide analysis tools for the design and evaluation of efficient low-noise rotorcraft, as well as to support the development of safe, low-noise flight procedures. CARMA consists of separate CFD (computational fluid dynamics), CSD (computational structural dynamics) and non-CFD rotorcraft performance, aerodynamic, wake and acoustic analysis programs, along with ‘interface’ codes to couple the separate analysis into a system capability. CARMA is in its initial stage of development and implementation. The analyses that are currently functional within CARMA are shown in Figure 1. This current system has basically four stages: (1) a comprehensive rotorcraft aeromechanics analysis to determine the trim state of the vehicle, (2) a high-resolution reconstruction method to compute high-resolution blade loading that is consistent with the low-resolution trim state, (3) a tone noise acoustic method which computes the acoustics on a noise hemisphere “near” the vehicle, and (4) a propagation method to compute the acoustics at distant observer locations while accounting for effects such as atmospheric attenuation and absorption, terrain, *etc.* The system is designed to predict the noise from fixed rotor systems, such as those in a wind tunnel as well as from rotorcraft in flight.

The CARMA prediction system starts with the definition of the rotor or rotorcraft system. The Comprehensive Analytical Model of Rotorcraft Aerodynamics and Dynamics (CAMRAD-II) [ref. 11] uses this definition to compute the rotorcraft trim state, which includes the rotor wake, rotor blade motion and rotor

airloads for a specified flight or wind tunnel condition. CAMRAD-II also includes a “post-trim” model to reconstruct and compute the high-resolution airloads and blade motion, which are required for input to the acoustic analysis. The CARMA interface codes, such as “user defined subroutine” and “setup_acoustic_calcs” aid in preparing the inputs to both CAMRAD-II as well as the acoustic and propagation analyses.

The first interface code, “setup_acoustic_calcs”, serves two purposes. First, it either extracts relevant data from the CAMRAD-II computations, or, alternatively imports data from an external source. Second, it interprets these data, and outputs relevant data to be used in the acoustic tone noise analyses WOPMOD or WOPWOP3. WOPMOD is a highly modified version of the original WOPWOP computer code [ref. 12]. WOPWOP3, also known as PSU-WOPWOP [ref. 13], also computes rotorcraft tone noise but does so in a far more general fashion than WOPMOD. WOPWOP3 uses its own internal data formats, so an additional interface code (“wopwop3-converter”) is used to convert data into a format compatible with WOPWOP3. Both WOPMOD and WOPWOP3 are based on the same acoustic formulations and for steady state flight or wind tunnel conditions give the same results. For the examples shown in this paper the WOPMOD analysis is used due to its current computational efficiency compared to WOPWOP3.

The high resolution airloads and blade motion along with the trim condition computed by CAMRAD-II are input to the acoustic analysis, which then computes the source noise at specified “observer” locations. For the wind tunnel case, observers are defined on a plane below the rotor. For the flight predictions the observers are defined on a constant-radius hemisphere surrounding the rotor being analyzed. The radius of the hemisphere is set to ten rotor radii for the predictions presented in this paper. This distance is far enough away from the rotor that the sound is traveling essentially perpendicular to the hemispherical observer surface, but is close enough that atmospheric effects are assumed negligible. For a multiple rotor vehicle, separate noise calculations are carried out on separate hemispheres – one for each rotor.

To compute the acoustics on the ground for a given flight operation, single or multiple sound hemispheres are used in the atmospheric propagation analysis Rotorcraft Noise Model (RNM) [ref. 14]. Either measured or predicted sound hemispheres may be used in RNM. RNM uses the sound hemispheres to compute noise at distant observer locations, while accounting for such effects as atmospheric absorption and attenuation, ground attenuation and reflection, terrain, flight track, *etc.* To prepare these sound hemisphere data for RNM, either the interface code “read_wopmod_array” or “read_wopwop3_array” is used, depending on whether WOPMOD or WOPWOP3 is used, respectively. These interface codes convert the noise hemisphere data into a NetCDF [ref. 15] format, as required by RNM. Comparison of acoustic metric histories at observer locations on the ground are made and presented using data from measured and predicted sound hemispheres.

Wind Tunnel Prediction

Wind tunnel test description

A complete description of the HART-II wind tunnel test is provided in reference 5, but a brief description is provide here for completeness. The HART-II wind tunnel test was conducted in the German-Dutch Wind Tunnel (DNW) in October 2001. This comprehensive measurement effort used a 40% dynamically- and Mach-scaled model of the BO-105 hingeless rotor system. The model rotor radius, R , was 2 meters. This test measured rotor vortex wake locations using 3-Component Particle Image Velocimetry (3C-PIV) and blade positions using Stereo Pattern Recognition (SPR). Balances measured gross rotor load parameters, while Kulite pressure sensors at several blade radial stations measured rotor aerodynamic loading. Also measured were the acoustics on a microphone plane located approximately $1.1R$ below the rotor hub. This measurement plane spanned approximately $2R$ fore and aft of the rotor hub, and approximately $1.35R$ laterally to either side of the rotor hub.

Predictions

Both references 16 and 17 use the full-span free wake model in CAMRAD-II to predict loading and acoustics for the HART-II model rotor. CAMRAD-II includes capabilities to model the wake with single or multiple trailers. The full-span wake model uses multiple trailed vortices in the far wake to model the spanwise distribution of vorticity, which would be an expected improvement over modeling the wake with the traditional single tip vortex model. This full-span trailed vortex wake model has been used with success in predicting rotor performance and airloads for tilt-rotor model rotors [ref. 18]. A more detailed investigation and validation of this wake model is beyond the scope of this paper, however such an investigation will be critical in the future

for improving predictions of the airloads for acoustics. Application of the full-span wake model combined with an adequate post-trim resolution is prohibitively expensive in terms of required computer memory and computational time. As such, only a single tip vortex model is computationally feasible in this study for these multi-rotor configurations using the current post-trim capability. Methods to alleviate this limitation are currently being considered for implementation within CARMA. However, to illustrate some of the sensitivity of the predictions to different wake models, the differences in predictions with the full-span wake model and the single tip vortex model are examined briefly for a BVI condition. The condition known as the “baseline” condition examined in references 16 and 17 is equivalent to a 6° descent at an advance ratio of 0.15 and rotor thrust coefficient (C_T) of 0.0044. Comparison of results from the full-span wake model and the single tip vortex model are shown for this baseline condition. These results illustrate the sensitivity of the airloads and acoustics to different wake models under this descent condition.

The full-span wake model [ref. 11] used here places a trailed vortex line at each aerodynamic panel edge in the far wake of each rotor blade. The reference blade for each rotor retains the “near-wake lattice” model [ref. 11]. The number and location of the aerodynamic panels are specified by the user, but are typically placed so that smaller panels (on the order of $0.02R$ in width) are at the blade tip. The aerodynamic panel size typically increases smoothly from the tip panels to the root panels. For the case presented here, sixteen aerodynamic panels are used, resulting in seventeen trailed vortex lines. The strength of each trailed vortex line is determined from the local aerodynamics where the vortex originates and the vortices are allowed to consolidate into a smaller number of trailed vortices as wake age increases. The default “single tip vortex model” places a single, constant core radius vortex at the tip of the blade with the vortex strength equal to the maximum bound circulation determined at the time of emission.

The rotor collective, lateral cyclic, and longitudinal cyclic pitch controls are adjusted simultaneously to achieve a specified thrust and to drive the two non-torque hub moments (perpendicular to the shaft axis) to zero. The first part of Figure 2 shows the measured and predicted loading at a radial station of $0.87R$ for both the full-span wake model and for the single tip vortex model. The black lines are the measured data; the red lines are the predictions. The predictions using these two models show the same general features as follows. In the first quadrant, between azimuth angles of 0° and 90° , measured blade vortex interactions (BVI) are seen as multiple pulses. The prediction shows the blade vortex interactions (BVI), but the BVI pulses occur slightly later in azimuth and have slightly different waveforms and amplitudes than the measured BVI pulses. BVI events can also be seen in the fourth quadrant. The prediction appears to compare with the retreating side BVI events, but the amplitudes of individual events are over-predicted and the pulse widths in the prediction are different from those in the measured data. The predictions using either wake model appear to lack many of the details seen in the measured data. Figure 3 shows the predicted $C_N M^2$ loading distribution over the entire rotor disk. The predicted BVI events can be seen in the first and fourth quadrants, corresponding to those seen in Figure 2. The similarity between the two predictions seems to suggest that these vortex line models alone cannot fully capture the details needed for acoustic predictions. This cannot be fully known until these wake models are more thoroughly assessed by comparing with detailed wake geometry measurements. To fully understand the effects of these differences, a much more thorough investigation of not only the wake geometry but also the full aeromechanics and structural mechanics needs to be assessed in order to further develop and validate the prediction capabilities.

The temporal and spatial derivative of loading is important for accurate noise predictions from BVI events. Figure 4 shows the distribution of the derivative of $C_N M^2$ loading with respect to time (at each radial station) over the rotor disk for the full-span wake model and the single tip vortex model. The locations of the BVI events are readily seen, as the regions of high gradients in loading contours. Since these two figures are very similar for the two wake models in this case, the noise predictions from these different wake models is expected to be similar. Figure 5 compares the measured mid-frequency sound pressure level in decibels (Mid-SPL [dB]) with predictions using the full-span wake model and the single tip vortex wake model. The Mid-SPL frequency range for this rotor covers the 6th through the 40th blade passage frequency (BPF) harmonics. With a BPF of approximately 69 Hz, the Mid-SPL range includes frequencies from approximately 414 Hz to 2760 Hz. This figure contains the contours of the Mid-SPL noise on a microphone array plane located below the rotor plane. For reference, the rotor diameter is represented on the plots by a black circle. The horizontal axis is the lateral location of the microphone relative to the center of the rotor hub. The vertical axis is the streamwise location of the microphone array, relative to the center of the rotor hub. The upstream and downstream locations are marked for reference. All plots of this type shown later follow this same format. The measured data shows the typical elevated noise levels on the advancing side under the rotor and on the retreating side under, and slightly behind, the rotor. The predictions show a similar trend, but the levels and details of the noise directivity

are not fully captured. Both predictions show advancing and retreating side BVI levels higher than the measured data. The location of the predicted advancing side BVI occurs farther forward than the measured location. This is consistent with the location of the loading shown in Figure 2, where the predictions of the BVI events occur at later azimuth angles than the measured loading indicates. The measured data also shows a rapid decrease in Mid-SPL noise not seen in the predictions. For the region that is forward of the retreating side, this may be in part due to acoustic shielding from the fuselage, which is not included in the predictions. However, this again indicates the inaccuracies and limitations of the current models to predict accurate airloads for BVI rotor conditions. As additional capabilities such as fuselage/sting aerodynamic interference effects, fuselage/sting acoustic shielding and scattering effects, advanced aerodynamic and wake modeling effects, blade elastic motion/acoustic effects, *etc.* are added to CARMA, these predictions are expected to improve.

Comparing the predictions from the two wake models, it is seen that they qualitatively give similar results. However, the predictions from using the full-span wake model have higher noise levels (approximately 1-2 dB) and larger BVI regions than those predicted using the single tip vortex model. Though the effects of the full-span wake model need to be examined in the future, the current modeling of multiple rotors is not computationally feasible with the current full-span model. Due to these computational limitations, the single tip vortex model will be used for the remainder of this paper.

Flight Prediction

Flight Test Description

This section will illustrate the flight prediction capabilities of the current CARMA system using a small subset of measured acoustic data from the Acoustic Week flight test program. Hardesty, *et al* [ref. 3] gives detailed description of the flight test setup; therefore, only a brief description of the test will be given here for completeness.

The Acoustic Week Flight Test Program was sponsored by the Chicken Little Program Office with participation from the U.S. Army's Joint Research Program Office, AeroFlightDynamics Directorate (JRPO-AFDD), Aviation Applied Technology Directorate (AATD), and the NASA Langley Research Center (LaRC). The primary purposes of the test were to (1) acquire a rotorcraft acoustic flight database for prediction code development and validation, and for development of low-noise flight procedures, and (2) characterize the acoustic signature for a variety of rotorcraft, including unmanned vehicles. Acoustic measurements were obtained with a distribution of ground and elevated microphones for development of measured source noise hemispheres. In addition, sound jury response data were collected, along with long-range acoustic data obtained from a smaller distribution of ground and elevated microphones co-located at the sound jury site.

For the noise hemisphere development data collection, all vehicles were flown through the microphone array in level flight at 150 and 250 feet altitude at velocities of 60, 80, 100, and 120 knots (or at the maximum airspeed that vehicle was capable of flying, V_{MAX} , whichever was smaller). The MD-520N was also flown in shallow 3° descents through the microphone array. The 150-foot altitude level flight runs were considered the primary runs since this flight altitude allowed the measurement of the full source noise hemisphere. The 250-foot flyovers were flown to assess the effect of altitude, and hence the angular measurement resolution [ref. 16], on the noise hemispheres. Multiple runs (up to 4) at each flight condition were made to improve the statistical confidence of the measured results. On average 20 runs were made per vehicle, which required approximately two hours of flight time.

Though data were measured for one prototype rotorcraft UAV (a 4-bladed developmental manned vehicle based on the Schweizer Model 269D helicopter), at the time of publication of this paper, the prediction model for this conventional rotorcraft had not been fully implemented in CARMA. However, the prediction model for the MD-520N has been fully implemented and is used here to illustrate the flight prediction capabilities of CARMA. Though this vehicle is generally larger than most conventional rotorcraft UAVs, scaling methods can be employed in a similar manner as done by Boyd, *et al* [ref. 16] to predict the acoustics from different vehicle sizes.

Acoustic Measurements

To measure the source noise hemisphere of each vehicle during this flight test, a U-shaped “goal post” microphone array was used. This array consisted of 20 microphones and is schematically shown in Figure 6. Twelve microphones were arranged on ground boards on a line perpendicular to the vehicle ground (and flight)

track, while four microphones were suspended from each of two cranes that were located 400 feet to either side of the flight track; the highest microphones were 175 feet above the ground. For this paper, only the data from three ground microphones are considered, as shown explicitly in the figure. Microphone 7 is located 174 feet to the right (advancing side) of the vehicle flight track. Microphone 10 is on the centerline of the flight track. Microphone 13 is located 149 feet to the left (retreating side) of the flight track.

Data Processing

At each microphone, the measured digital acoustic time domain data were transformed to the frequency domain using the average of five 4096-point Fast Fourier Transforms (FFT) with a Hamming window and 50% overlap applied, resulting in 0.5120-second data blocks. Averaged narrowband spectra were computed beginning every 0.5 seconds for each microphone for the duration of each run and were then subsequently integrated. This integration produced OASPL noise metrics at each microphone location as a function of time. For the purposes of this paper, these integrated OASPL noise metric time histories at microphones 7, 10, and 13 will be used for comparison with predictions from CARMA. In addition to these narrowband spectra, one-third octave band spectra were also computed at each microphone. Subsequently, the Acoustic Re-propagation Technique (ART) [ref. 19] was used to generate the “measured” one-third octave band source noise hemispheres for a given flyover.

Results: Measured vs. Predicted OASPL During Flyover

A full vehicle of the MD-520N was modeled within the CARMA system. Specifically, the comprehensive analysis, CAMRAD-II, was used and included a detailed description of the main rotor and an aerodynamic representation of the tail force. The main rotor is fully-articulated and has five blades with a radius of approximately 13 feet 8 inches, a mean chord of approximately 7.1 inches, and a non-linear twist distribution. The airframe aerodynamics is modeled using an input table of lift force, drag force, side force, pitching moment, rolling moment, and yawing moment as a function of angle of attack, side-slip angle, and elevator angle. The horizontal tail aerodynamics is also modeled using an input table of lift and drag forces as a function of angle of attack. The MD-520N rotorcraft has a “NO Tail Rotor” (NOTAR) tail boom system which provides anti-torque. Aerodynamics of the NOTAR system is modeled using tables for lift and drag coefficients on the tail boom as a function of angle of attack and blowing coefficient. The blowing coefficient is further tabulated as a function of the pilot pedal displacement (*e.g.*, percent of full displacement) and velocity. All of the above tables were generated using the FLYRT code (see “Acknowledgements”).

Two cases are considered here. The first is a level flyover and second is a 3° descent. Using the model above in CAMRAD-II, trim solutions were obtained for both the steady-state level flyover condition and the 3° descent condition. Using WOPMOD, the tone noise was computed on a lower hemisphere under the rotor at a radius of ten rotor radii. The tone noise hemisphere predictions were then used in RNM to compute the Overall Sound Pressure Level (OASPL) noise metric time histories at the ground locations corresponding to microphones 7, 10, and 13. The OASPL metric was chosen since the rotor acoustics for the cases considered are dominated by the low frequency component of the noise. Note, the previous example for the wind tunnel 6° descent case was dominated by the higher frequency BVI noise and hence the mid-SPL metric was used for illustration.

Figure 7 shows measured and predicted OASPL metric time histories at the three microphone locations for a 150-foot level flyover at 80 knots. The horizontal lines in the graphs are time, in seconds, relative to the time when the vehicle is directly above the center microphone of the microphone array. Negative numbers indicate the vehicle is approaching the array; positive numbers indicate the vehicle has already past over the array. (For reference, at ± 20 seconds and 80 knots airspeed, the vehicle is located approximately 2700 feet horizontally (0.51 miles) from the centerline microphone, or approximately 3° above the horizon relative to the centerline ground microphone position.) The vertical axis is the OASPL [dB]. The black lines represent measured data. Multiple measured data lines are plotted from repeated runs and show that the measured data is highly repeatable. The red lines indicate the prediction.

It can be seen that the predicted noise level histories as a function of time show good agreement with the measured data between the ± 20 seconds relative to the overhead time, with the exception of the predicted peak levels. The origin of the elevated noise levels in measured data between the -40 to -20 seconds before overhead time frame appears to be from thickness noise (rotor in-plane noise), which is known to be sensitive to atmospheric propagation effects. Further investigation is needed to fully understand the exact cause of these

elevated levels. A constant noise level is seen in the measured data starting at about 25 seconds after overhead. This constant noise level indicates the ambient noise level during this run. The peak levels are under-predicted by about 5 dB at the centerline microphone and about 10 dB at the retreating side microphone, while the advancing side peak is over-predicted by about 5 dB. To investigate this, more detailed measurements of the rotor airloads and vehicle trim are needed. It is speculated that these under- and over-predictions are due to a combination of factors. These factors can include differences between the nominal flight track used in the predictions and the actual flight track flown as well as other effects due to weight and trim variations and wind effects, *etc.* In addition, the CARMA code does not currently include rotor broadband or non-rotor noise sources such as engine noise, *etc.* For the MD-520N, there are several of these noise sources (engine noise, anti-torque tail boom noise, *etc.*) that are not currently taken into account.

In the level flight case, within the ± 20 seconds window, the mean airspeed and altitude matched the nominal, or requested, conditions well. The deviations in the mean airspeed were within $\pm 2.5\%$, or ± 2 knots, of the nominal value. The deviation mean altitude was within approximately $\pm 10\%$, or ± 15 feet, of the nominal altitude. With respect to the lateral location, the actual flight path was within approximately ± 15 feet of the nominal flight track. However, for this descent case, there were some average offsets (mean deviations) in airspeed and altitude from the nominal values. For example, Figure 8 shows the requested (or nominal) and measured altitude and airspeed for the descent case. Also shown are the values that were used in the predictions. To account for these mean offsets, noise predictions for this descent case were made using 85 knots airspeed and the altitude profile shown in Figure 8. Figure 9 shows the same predicted and measured noise quantities as in Figure 7, but for the 3° descent case. The prediction comparison to measurement is similar to that for the level flight condition. CARMA over-predicts the peak levels for the centerline microphone (about 3 dB) and the advancing side microphone (about 6 dB). The overall shape of the predicted noise compares quite favorably with the measured data between approximately -20 to +10 seconds from the overhead position. These examples are used to illustrate the current capabilities of CARMA to predict flight noise and for initial assessment of how well the predictions compare with available measured data for a level flight condition as well as a mild descent condition. To fully validate such a prediction analysis, data for other flight conditions are needed and more detailed measurements of the rotor aeromechanics and vehicle dynamics are required.

Coaxial Rotor Aeroacoustic Analysis

The two most abundant types of open-rotor, rotorcraft UAVs use either a conventional rotor system or a coaxial rotor system. The conventional rotorcraft UAV system is comprised of a main rotor and (typically) a tail rotor and appears similar to many of the conventional manned rotorcraft vehicles in flight today. Coaxial UAV rotor systems, on the other hand, consist of two main rotors that are counter-rotating, which eliminates the need for an anti-torque device. Conceptually, an acoustic flight prediction for a coaxial system could follow the same steps as done for a conventional system, as demonstrated for the MD-520N earlier. Though measured acoustic signatures have been obtained for some vehicles [ref. 10], an open literature search reveals little work has been done on acoustic prediction methods for coaxial rotor systems. The current CARMA system is used to illustrate its capabilities in modeling and predicting the noise from a notional coaxial rotor system.

The model BO-105 rotor used in the HART-II test is used to create a “baseline coaxial” rotor system. Two isolated BO-105 rotors are placed vertically on a common rotor rotational axis. The thrust of each rotor is that of the isolated BO-105 rotor, hence the total coaxial rotor system has twice the thrust of the isolated rotor. The total non-torque hub moment of the two rotors is trimmed to zero at the center of the rotor system. The separation distance between the two rotors is varied to allow for examination of aeromechanic and acoustic interaction effects as a function of rotor separation distance. For all the examples presented the rotors are phased such that they co-align when one of their respective blades are at zero azimuth. The baseline HART-II 6° descent condition is used for these illustrations; hence, the acoustic results are presented using the Mid-SPL noise metric.

Non-interacting rotors with vertical separation

When examining coaxial counter-rotating rotors, there are two possible rotation configurations. When looking from above, the lower rotor can rotate counter-clockwise while the upper rotor rotates clockwise and visa versa. Only one configuration needs to be modeled since results for the other configuration can be obtained by rotating the noise plots 180° about the streamwise axis. For this illustration, the lower rotor rotates counter-clockwise and the upper rotor rotates clockwise. Also, the illustrations shown in this paper only consider one

phase angle between the two rotors, realizing that the phasing of the rotors can greatly affect the radiated noise directivity and levels. The phase angle chosen is such that the blades are aligned at an azimuth angle of zero degrees ($\psi = 0^\circ$). While practical vertical rotor separation distances for current vehicles are on the order of 0.25R, vertical separations over a much wider range are considered in this study to investigate the effects on the noise. Five are examined here: 0.00R, 0.25R, 0.50R, 0.75R, and 1.00R. These vertical separations are achieved by keeping the lower rotor fixed at its original location and moving the upper rotor upward. No aerodynamic interactions between the two rotors are considered here.

Figure 10 shows the Mid-SPL noise results for the range of vertical rotor separation distances. For the vertical separation equal to zero, the expected symmetric noise directivity is seen. For this case, the maximum Mid-SPL levels are about 2-4 dB higher than the other cases where the rotors are vertically separated. As the vertical separation distance increases the noise directivity pattern changes due to the phasing of noise from each rotor. The prediction technique sums the acoustic pressure time histories to preserve the phase between the acoustic pressures from each rotor as each signal reaches each observer. This approach, instead of adding on a “p-squared” basis, preserves the acoustic interference between two (or more) rotors when the pressure time histories cover comparable frequency ranges; this technique is applicable to multi-rotor configurations (*e.g.*, tilt-rotor, coaxial, tandem, and intermeshing configurations). The maximum levels are partly reduced as the separation distance increases, since the upper rotor is farther from the observer than when the vertical separation distance is zero. It is also interesting to note that these non-zero separation cases have Mid-SPL maximum noise levels which are comparable to the isolated rotor case. However, in general, noise levels are sustained at higher levels over a larger area when compared to the isolated rotor case, which is expected since the thrust is twice that of the isolated rotor case.

Aerodynamically Interacting Rotors

Aeromechanic Analysis

The previous sections examined the acoustics from two independent, non-interacting rotors. Aerodynamically, however, these two rotors will interact to some degree, especially when the rotors are in close proximity to one another. To analyze the two-rotor interacting system, a modified coaxial rotor system was used in CAMRAD-II. The trim procedure in CAMRAD-II was set up so that the collective, lateral, and longitudinal pitch controls operated as usual on each of the rotors. These three pitch controls were used to trim three quantities to target values (*i.e.*, “trim targets”). The first trim target was again set such that the total thrust from the two rotors was equal to twice the isolated rotor thrust. Since these two rotors are interacting, the thrust on each rotor is not required to be the same; it is only required that the total thrust equal twice the isolated rotor thrust. The next two trim targets were designed so that the two net (non-torque) moments at a point mid-way along the shaft axis between the two rotors are each zero. In the isolated rotor case, these “hub moments” were trimmed to zero. Since only the net moment of the two rotors is required to be zero, each rotor can have a non-zero moment.

In the CAMRAD-II analysis, the rotors are allowed to interact aerodynamically such that the aerodynamics at each aerodynamic “collocation point” on one rotor is influenced by the non-uniform induced velocities from the other rotor. Since the aerodynamics of each rotor will be different due to these mutual interactions, the blade motions and wakes of each rotor will also be different. The only interacting effect that is not taken into account for these calculations is the direct influence of one rotor’s wake induced velocity on the other rotor’s wake geometry. The wake geometry of each rotor is however indirectly influenced by the other rotor’s wake. This indirect influence comes through changes in each rotor’s blade circulation, blade motion, and final rotor trim state (of each rotor) caused by the mutual aerodynamic interferences on the rotor blades.

For this section, the coaxial rotor system is examined for each of the non-zero rotor separation distances shown for the “non-interacting” predictions. Compared to the non-interacting cases, the predictions for each case are trimmed separately. Examining the aerodynamic loading and the Mid-SPL noise contours for each rotor for the various vertical separations shows the effects of aerodynamic interferences.

Aerodynamic loading

In a manner similar to Figure 2, the aerodynamic loading is examined for a range of rotor vertical separation distances. Figure 11 shows the $C_N M^2$ aerodynamic loading at the radial station of 0.87R for both the lower and upper rotors as function of azimuth angle. Note that, since the rotors are counter-rotating, the azimuth angle is measured in the direction of rotation for the respective rotors. Each rotor has different $C_N M^2$

distributions. The differences are most pronounced for the smaller rotor separations. Due to mutual interferences, these two rotors are in separate states of trim; each of which is different from the isolated rotor trim state shown in Figure 2. For example, the isolated rotor was trimmed to have zero hub moments. Each of these interacting rotors has a non-zero set of hub moments. These interacting rotor trim states are a complicated combination of trim parameters that are determined during the iterative trim process within CAMRAD II. Figure 12 shows the variation of thrust coefficient and coning angle as a function of rotor vertical separation distance. For reference, the isolated rotor values are also shown. (The isolated rotor value is the one that was used for the non-interacting and for the isolated rotor cases.) Relative to the isolated rotor value, the lower rotor is shown to be operating at a higher thrust level, while the upper rotor is operating at a lower thrust level. As the rotor separation distance increases, the thrust on each rotor approaches the isolated rotor value. However, even at the separation distance of 1.00R, the thrust from each rotor is not the same. This indicates that each rotor still has significant influence on each others' overall trim state. The coning is also seen to be different on each rotor, though the figure is plotted on an expanded scale. At a rotor separation of 1.00R, there is only a small difference in the coning values of each of the rotors, and the coning on both the upper and lower rotors approaches the isolated rotor value asymptotically.

Another indicator that can be used to assess the level of interaction between the rotors is the induced inflow from one rotor on the other. Figure 13 shows two of the components of mean interference inflow ratio on each rotor. The mean interference inflow ratio is defined as the mean inflow ratio component (*i.e.*, inflow velocity divided by the rotor tip speed) on one rotor that was caused by the presence of the other rotor. Figure 13 shows both the λ_{XINT} and the λ_{ZINT} components of mean interference inflow ratio. The λ_{XINT} component is parallel to the tip path plane and is positive in the aft direction. The λ_{ZINT} component is normal to the tip path plane and is positive in the positive thrust direction. It can be seen that the lower rotor induces an additional streamwise component of velocity on the upper rotor while the upper rotor induces an additional inflow in the opposite direction (*i.e.*, forward). In addition, the lower rotor induces a larger additional vertical inflow component on the upper rotor than the upper rotor induces on the lower rotor. This inflow trend appears nominally consistent with the measured trends discussed by Coleman [ref. 20] that the vortices from the upper rotor typically have a higher convection speed than those of the lower rotor. With regard to the horizontal (in-plane) component of interference inflow, Coleman [ref. 20] states that, "Omission of the longitudinal inflow variation in some cases leads to large errors". In the current CARMA method, this component (and the lateral component as well) is included in an implicit manner.

Examination of the thrust, coning, and mean interference inflow components above are a small part of the trim analysis. These effects were examined here for illustration and to begin exploration of the limitations, strengths, and weaknesses of the prediction capabilities currently in CARMA. Further examination the prediction models and comparison with measurements is needed to fully assess and improve the capabilities.

Mid-SPL Noise

The noise directivity contours of Mid-SPL for increasing vertical rotor separations are shown in Figure 14. In the 0.25R separation case, two main noise directivity regions can be seen. The lobe on the right side is mostly attributable to the blade-vortex interactions (BVI) events in the first quadrant of the lower rotor; the lobe on the left is most attributable to the BVI events in the first quadrant of the upper rotor. Several factors contribute to the fact that the right side lobe is stronger than the left side lobe. First, the BVI events on the lower rotor are stronger than those on the upper rotor, and second, the lower rotor is closer to the observer plane. With increased vertical rotor separation, the primary noise directivity pattern remains nominally the same in that, essentially one main lobe remains on each side of the rotor system. For the larger separations, the lobe attributable to the upper rotor is diminished in strength because the distance between the observer plane and the upper rotor is increased, and the overall directivity pattern appears to be approaching that of an isolated rotor with one main lobe on the right side of the system. For this 6° descent condition, the predicted directivity patterns for the non-interacting and the interacting rotor cases are substantially different for all rotor separation distances. Thus, the rotor interference effects (aerodynamic and acoustic) appear to be significant. To fully understand and verify these results, comparison with experimental data is needed.

Coaxial Rotor System vs. Single Rotor System

The basic CARMA system provides computational tools that can be used for initial assessment and comparison of different rotorcraft configurations. An example comparison is provided in this section to

illustrate how the CARMA system can be used to examine or compare different rotor designs. In this example, prediction of the Mid-SPL noise from the HART-II single rotor system is compared to a coaxial rotor system with a rotor separation of $0.25R$ and the same total thrust as the single rotor system. The coaxial rotor system is constructed exactly as described above and the predictions include the interaction effects between the two rotors.

Figure 15 shows the predicted loading ($C_N M^2$) at the radial station of $0.87R$ for each rotor in the coaxial system along with that from the single rotor system. The mean loading on each of the coaxial rotors (upper and lower) is approximately one-half of the mean loading on the single rotor. In addition, for the coaxial rotors, it can be seen that in the first quadrant of each rotor, there appears to be more significant BVI events than seen for the single rotor system. The predicted loading for each rotor in the coaxial system is different as a result of the interaction of the two rotors on each other. Even though each rotor is predicted to have less mean thrust than the single isolated rotor, it is expected that there will be more BVI noise generated with this coaxial system than with this isolated rotor case due to the more significant BVI events seen in the loading.

Figure 16 shows the noise prediction comparison between the single rotor system (same as shown in Figure 5 for the “Predicted single vortex model”) and the coaxial rotor system for equal thrust levels. The coaxial system has two regions where the Mid-SPL is high: one on the advancing side, the other on the retreating side. Both of these regions are higher in level than the maximum levels seen for the single rotor system. The loading from each rotor indicates that the Mid-SPL region on the advancing side is mainly due to the lower rotor, which is rotating counter clockwise and that the Mid-SPL on the retreating side is mainly due to the upper rotor, which is rotating clockwise. The single rotor system has the highest Mid-SPL noise level on the right side (advancing side) of the rotor and slightly forward of the rotor center. To verify these results, measured acoustic and aeromechanics data are needed; however, the predictions appear to capture many of the first order effects.

Summary

The emerging Comprehensive Analytical Rotorcraft Model for Acoustics (CARMA) prediction system has been described. It currently includes four basic analysis steps: (1) comprehensive aeromechanics analysis, (2) high resolution reconstruction, (3) rotor tone noise calculations, and (4) acoustic propagation to distant observers, which includes atmospheric and ground effects, among others. Using the current CARMA system, high resolution rotor loading and noise predictions were illustrated for an isolated rotor in a wind tunnel and comparisons were made with measured data. The predictions showed similar trends, but the levels and details of the noise directivity were not fully captured. CARMA flight prediction capabilities were illustrated by comparing predicted and measured noise metrics for the MD-520N rotorcraft. The comparisons were made at selected ground locations for level flight and mild descent conditions. The measurements were obtained from a flight test conducted in 2003 at Eglin Air Force Base. For the flight conditions shown, the predictions showed reasonable comparison with the measured data, except when the vehicle was directly over the microphone array, where noise levels were either over- or under-predicted depending on location. In part, this can be attributed to lack of accurate data defining the vehicle orientation and detailed trim parameters, as well as limitations in the prediction capabilities to include broadband rotor noise sources and other non-rotor noise sources (*i.e.*, NOTAR tail force, engine noise, *etc.*)

To illustrate the prediction versatility of the current CARMA system, acoustics from a notional coaxial UAV-sized rotor system were examined using two methods. The first showed the combined Mid-SPL noise from two aerodynamically non-interacting, isolated rotors. The second method showed the combined Mid-SPL noise from two aerodynamically interacting, isolated rotors. Aerodynamic loading for the interacting rotors was shown to be substantially different in the first quadrants of each rotor. These differences were more pronounced when the two rotors were in closer proximity to each other and diminished as rotor separation distance increased. As the rotor separation increased, the noise influence of the upper rotor diminished. These loading and acoustic differences show that it is important to account for mutual interferences between the rotors, especially when the rotors are in relatively close proximity. While a detailed study of these effects was beyond the scope of this paper, a more in-depth examination – analytically and experimentally – is needed to fully explore, assess, and understand the effects of these interactions and their influence on vehicle acoustics.

A representative type of comparison was also illustrated between an isolated rotor and a notional coaxial system with the same thrust and with a coaxial vertical rotor separation of $0.25R$. Though the mean thrust on each of the coaxial rotors was approximately one half that of the isolated rotor thrust, the notional system was predicted to generate more Mid-SPL noise than the isolated rotor. Though this is not a complete

design study, it demonstrates how the CARMA system could be used to compare configuration differences in such a design process.

Acknowledgements

The authors would like to thank Bruce Charles at The Boeing Company in Mesa, Arizona for providing the CAMRAD-II input deck – including airframe aerodynamic and NOTAR tables generated by the FLYRT code – for the MD-520N used in this work.

Figures

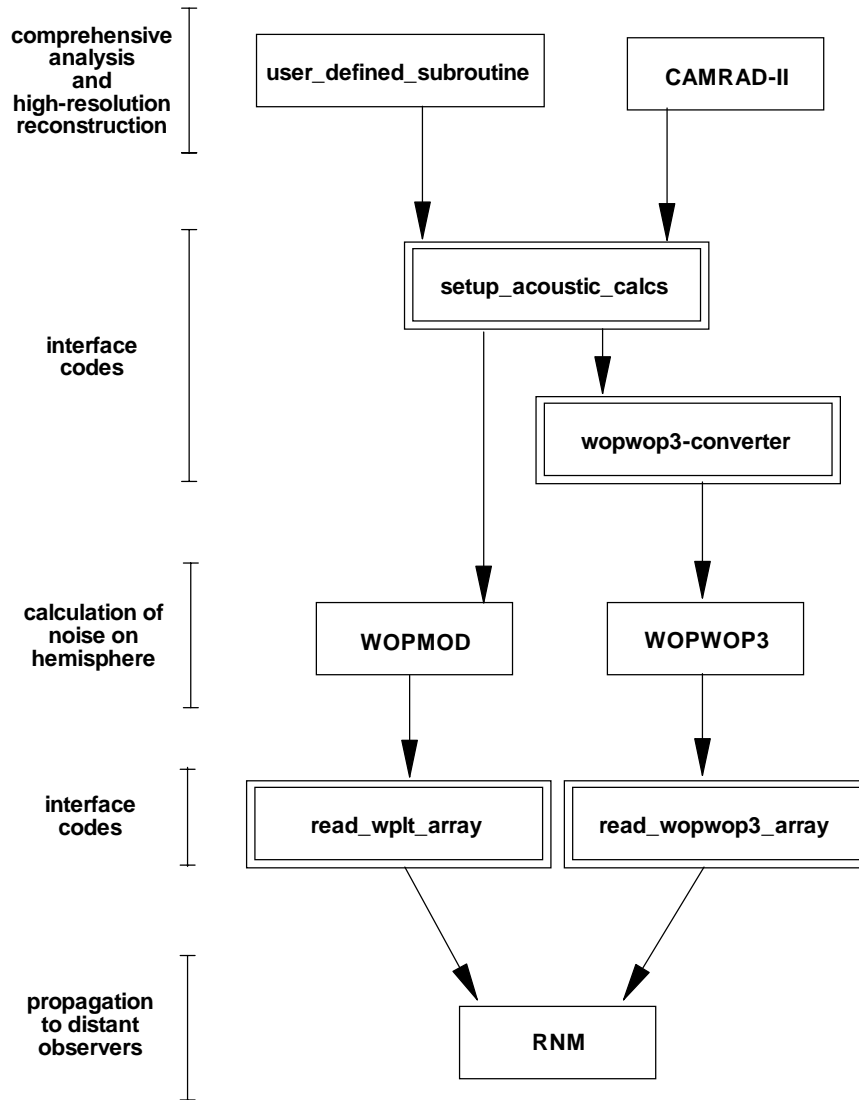


Figure 1: Outline of the initial Comprehensive Analytical Rotorcraft Model for Acoustics (CARMA) code.

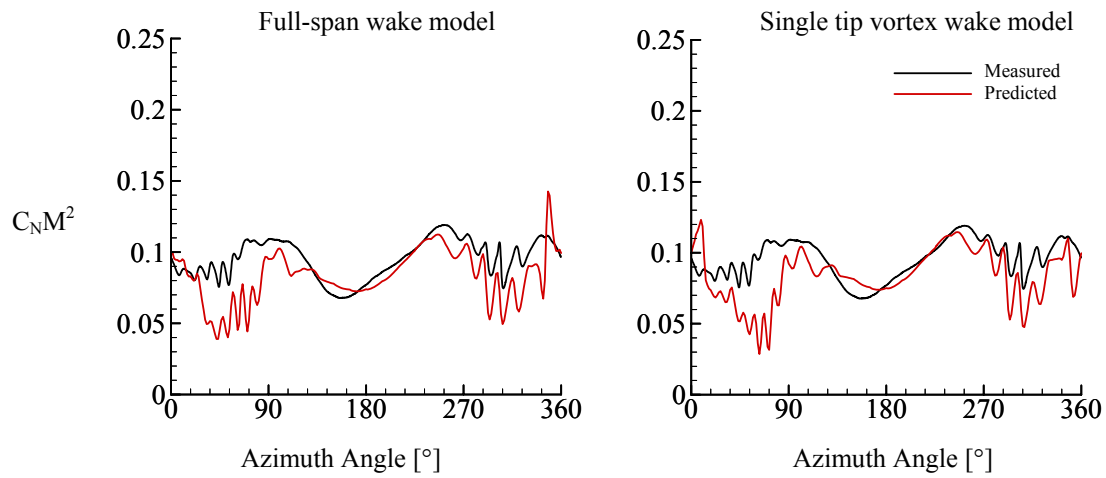


Figure 2: Measured and Predicted $C_N M^2$ loading at $r/R = 0.87$ from the isolated, HART-II model rotor in the DNW for the baseline case. Black lines represent measured data. Red lines represent predictions.

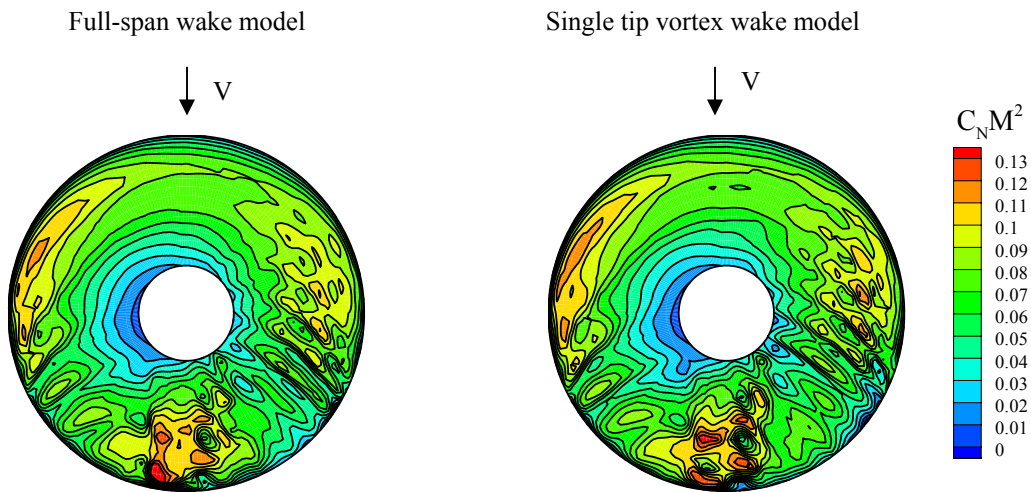


Figure 3: Predicted contour maps of $C_N M^2$ over the rotor disk for predictions of the baseline case utilizing the full-span wake model and the single tip vortex model.

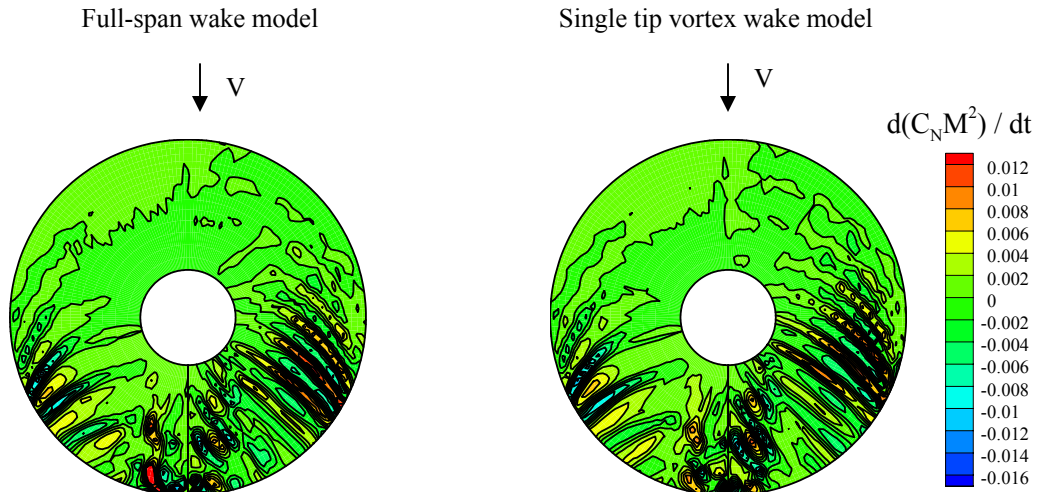


Figure 4: Predicted contour maps of $d(C_N M^2)/dt$ over the rotor disk for predictions of the baseline case utilizing the full-span wake model and the single tip vortex model.

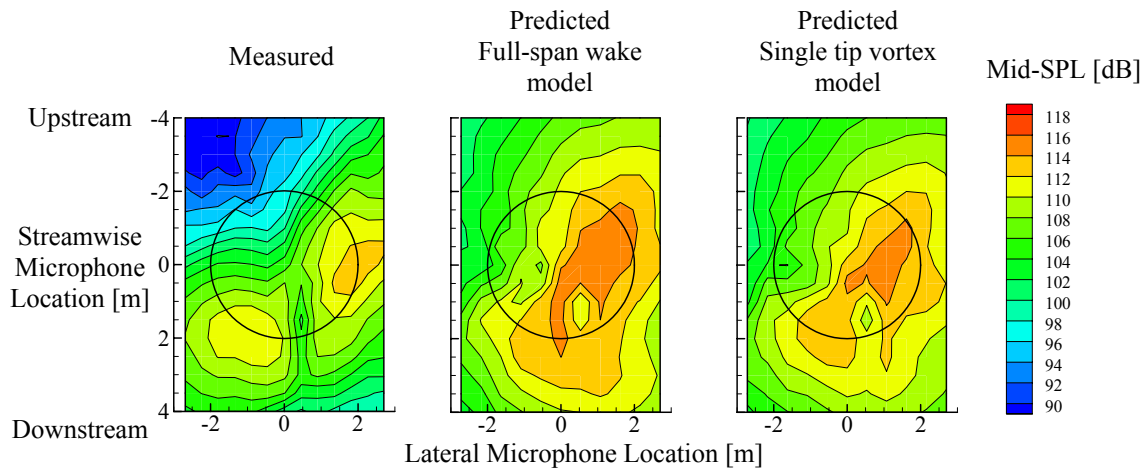


Figure 5: Measured and predicted noise directivity maps of Mid-SPL from the HART-II model rotor in the DNW for the baseline case.

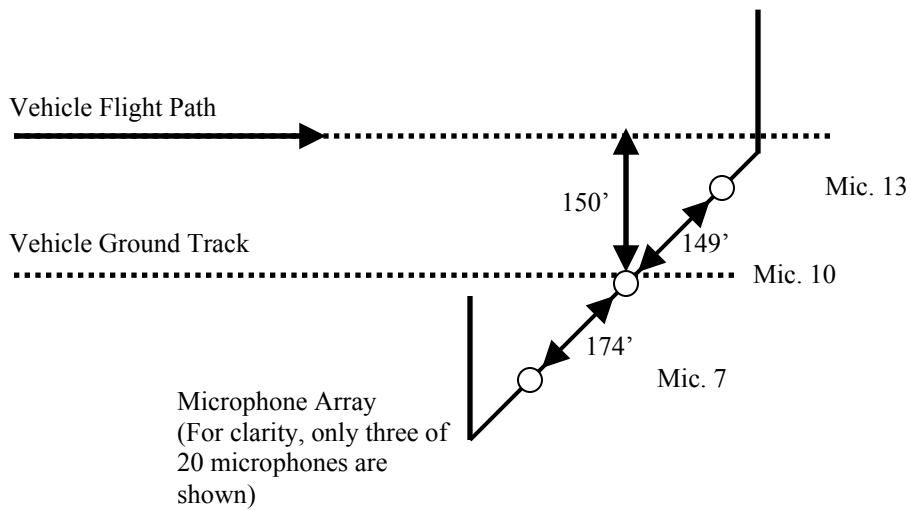


Figure 6: Schematic of the flight track and microphone array configuration used to obtain the data of the MD-520N in a level flyover at 150 feet.

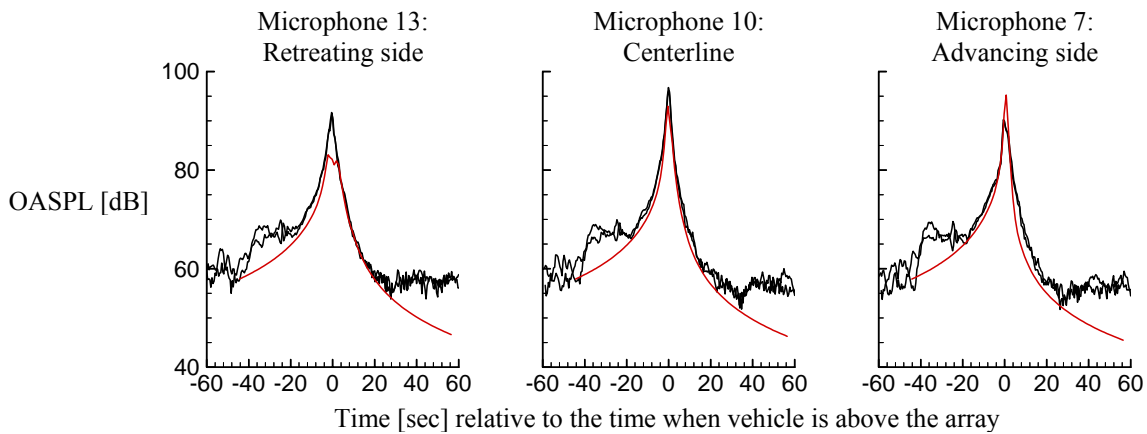


Figure 7: Comparison of measured and predicted OASPL [dB] histories from three microphone locations for the MD-520N vehicle in level flight at 80 knots. Black lines are measured data from repeated flights. Red lines are predictions using the CARMA system.

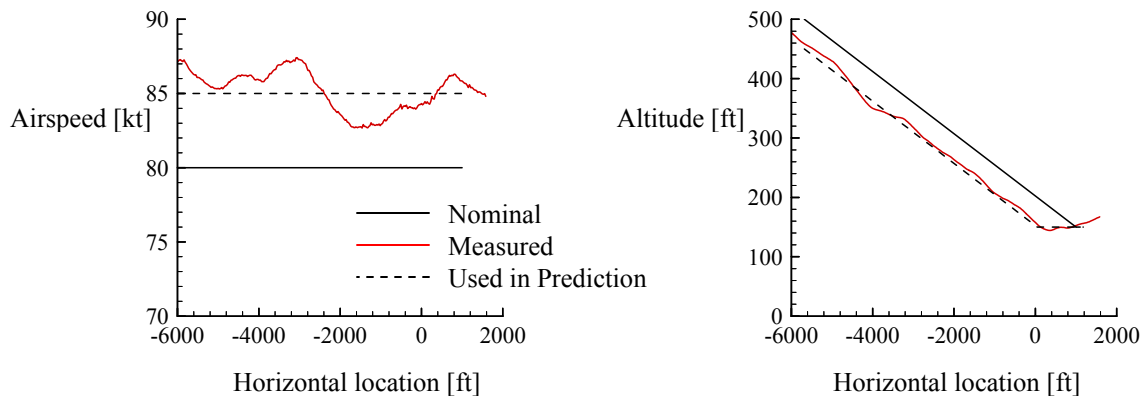


Figure 8: Airspeed and altitude data for the 3° descent flight condition of the MD520N. “Nominal” line is the intended airspeed and altitude profile. “Measured” line is the measured airspeed and altitude determined from the measured tracking data. “Used in Prediction” line is the value used for CARMA flight predictions.

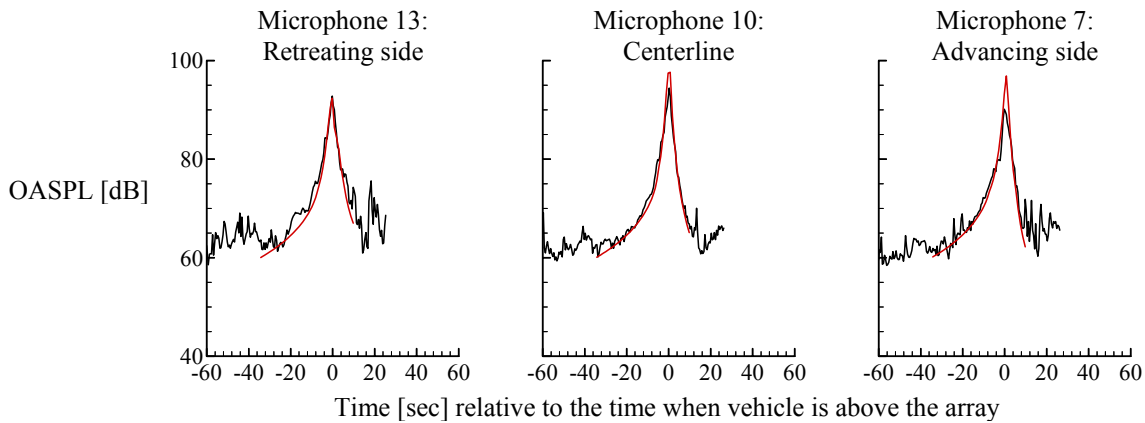


Figure 9: Comparison of measured and predicted OASPL [dB] histories at three microphone locations for the MD-520N vehicle at 85 knots in a 3° descent. Black lines are measured acoustic data from repeated flights. Red lines are acoustic predictions using the CARMA system.

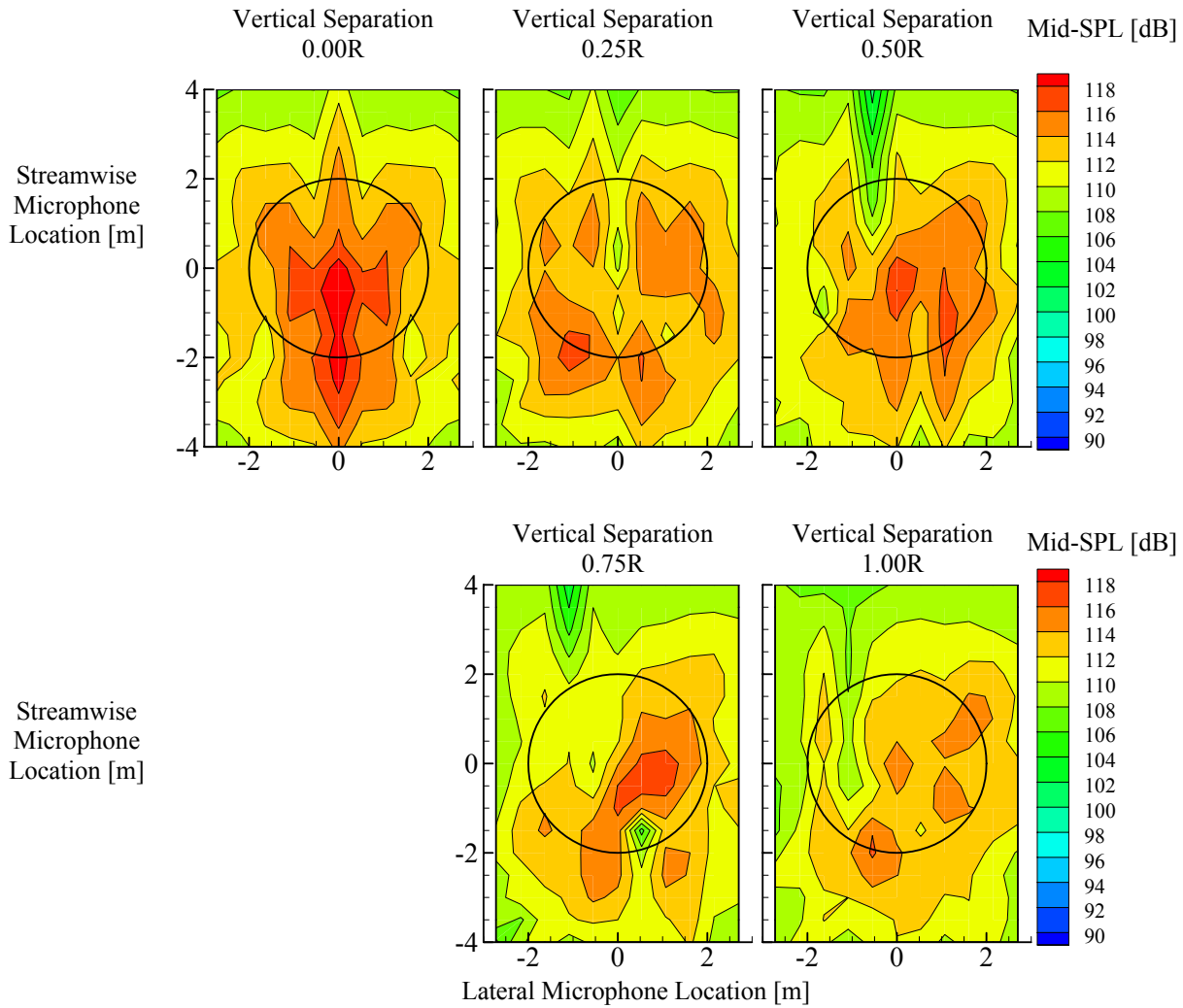


Figure 10: Predicted noise directivity of Mid-SPL determined for the aerodynamically non-interacting coaxial rotor system for different rotor vertical separation distances.

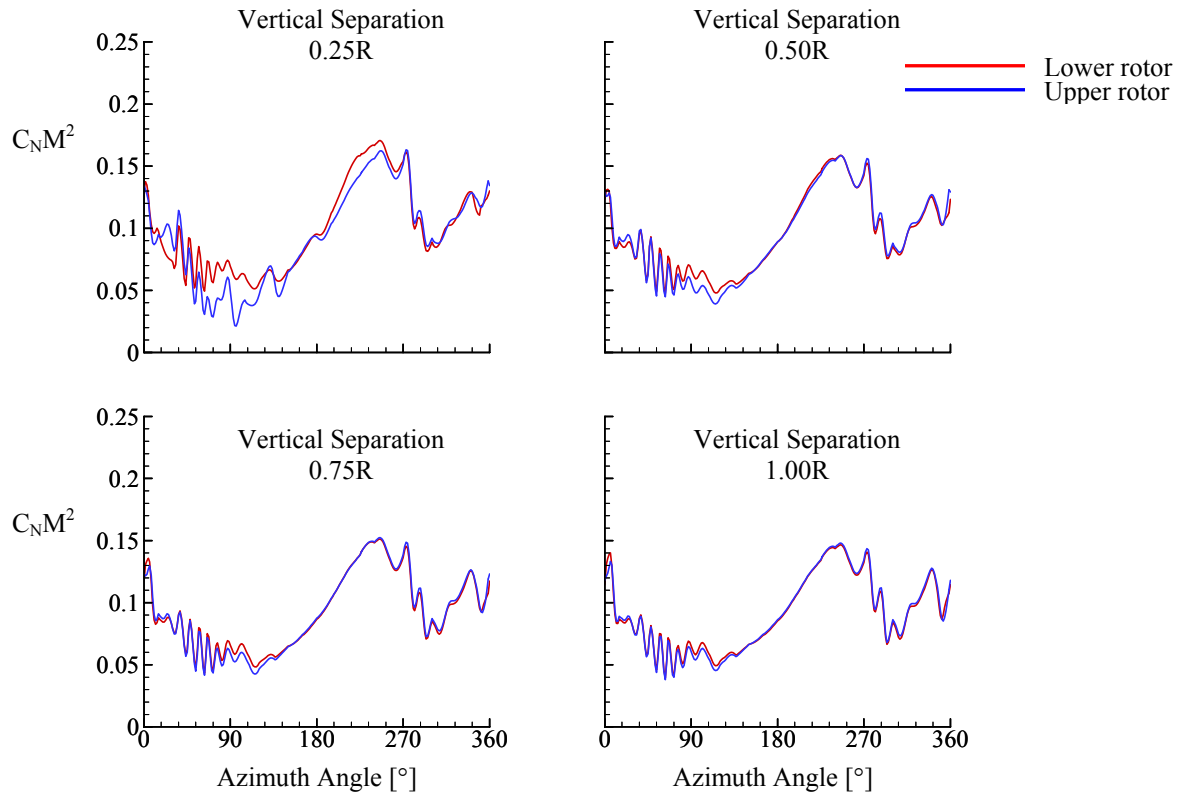


Figure 11: Predictions of $C_N M^2$ loading at $r/R = 0.87$ that include the effects of aerodynamically interacting coaxial rotors with varying vertical separation distances. Azimuth angle is measured in the direction of rotation for each rotor. Lower rotor rotates counter clockwise, upper rotor rotates clockwise.

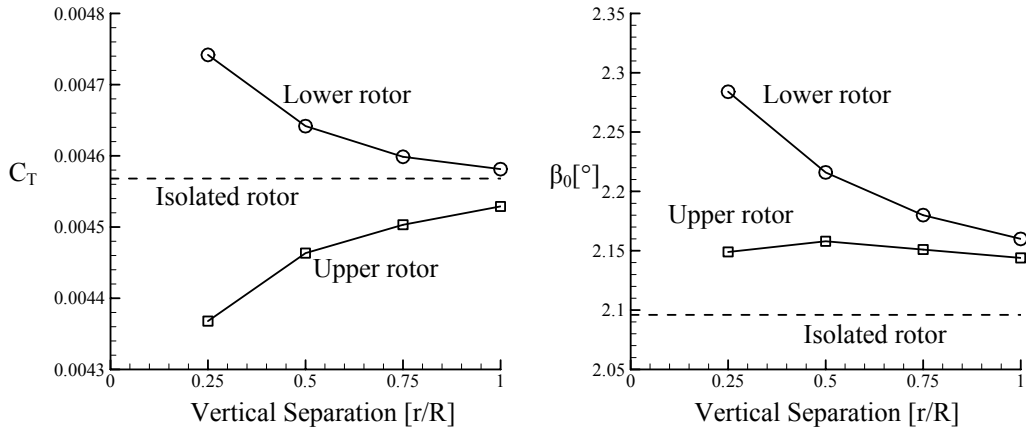


Figure 12: Thrust coefficient (C_T) and coning angle (β_0) for single rotor (dashed line), and coaxial rotor system: lower rotor (circle symbols), and upper rotor (square symbols).

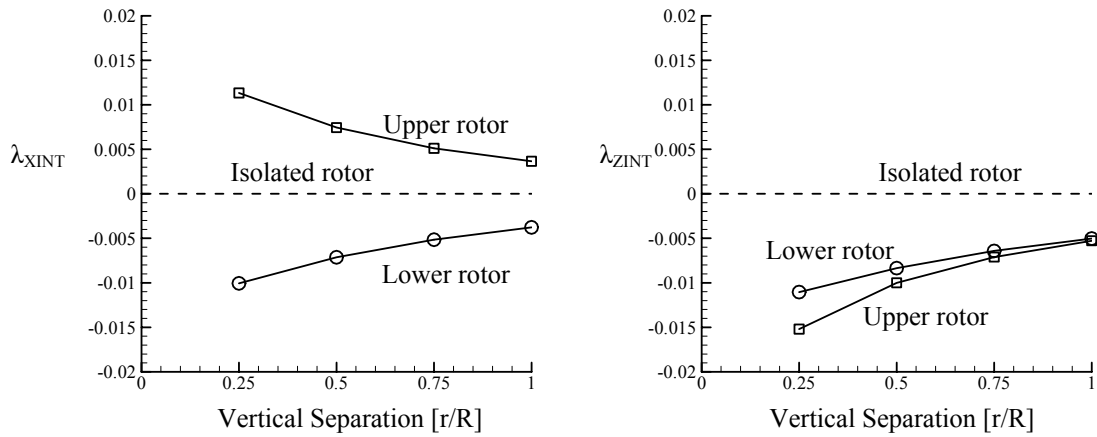


Figure 13: Mean interference inflow ratio (velocity divided by rotor tip speed) components: λ_{XINT} is the horizontal component in the tip path plane (positive aft); λ_{ZINT} is the vertical component normal to the tip path plane (positive in the thrust direction). The lower rotor is designated with circle symbols; the upper rotor is designated with square symbols.

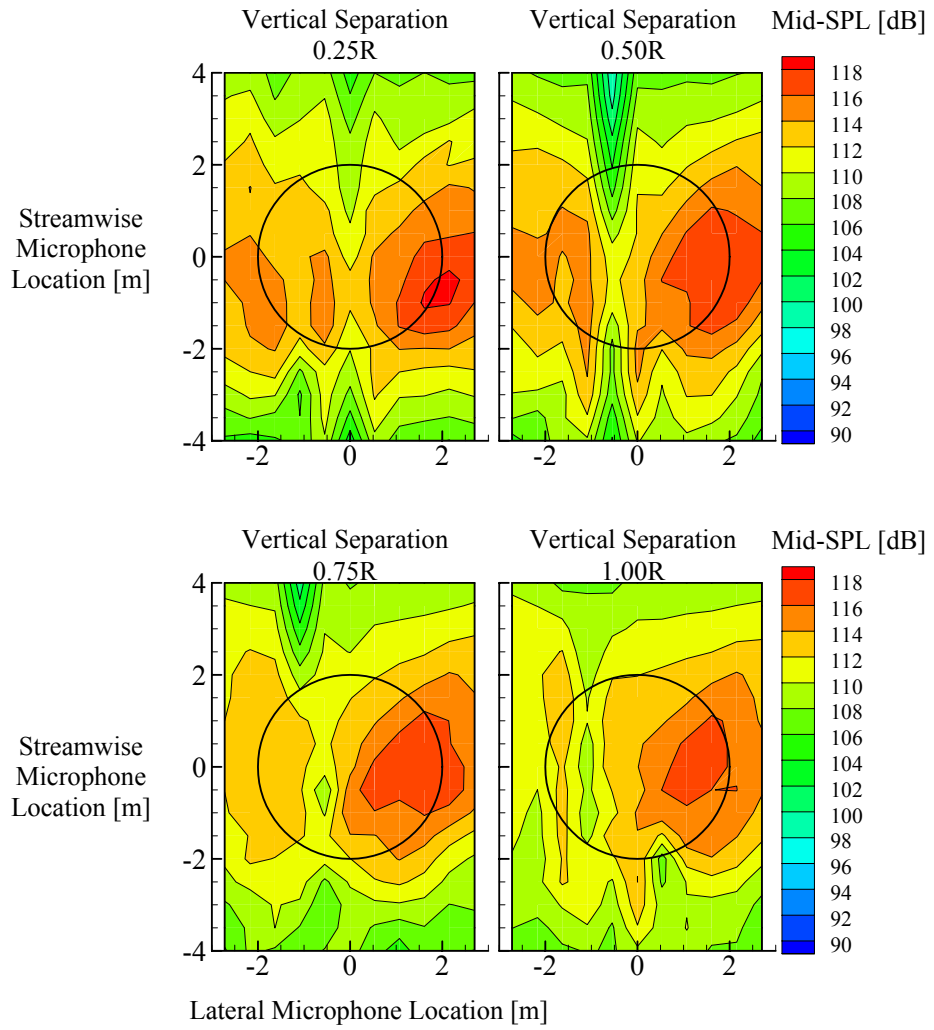


Figure 14: Predicted noise directivity maps of Mid-SPL for the interacting, coaxial rotor system at varying vertical rotor separations.

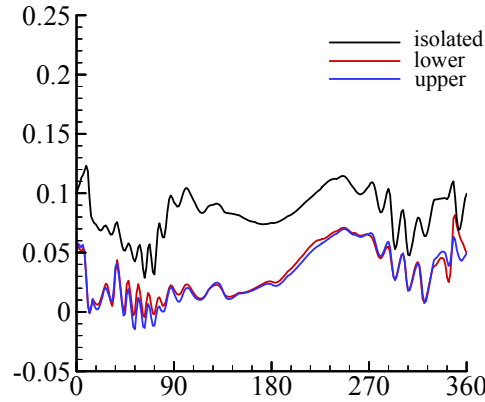


Figure 15: Comparison of $C_N M^2$ loading at $r/R = 0.87$ predicted for the isolated rotor and those predicted for each of the rotors in the coaxial rotor system. The notional coaxial system is trimmed to the same thrust as the isolated rotor ($C_T=0.0044$).

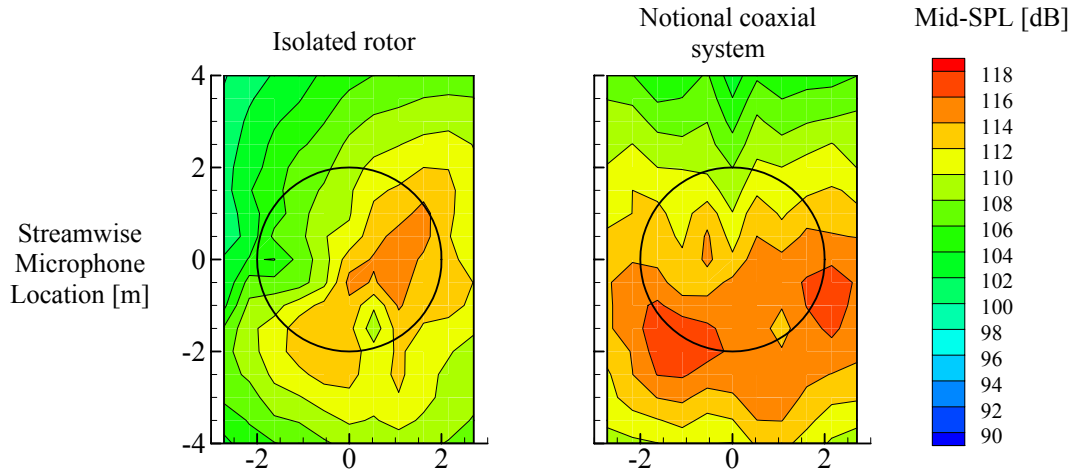


Figure 16: Predicted noise directivity of Mid-SPL determined for the isolated rotor and the notional coaxial system. The notional coaxial system is trimmed to the same thrust as the isolated rotor ($C_T=0.0044$).

References

1. Conner, D.A., Marcolini, M.A., Edwards, B.D., Brieger, J.T.: "XV-15 Tiltrotor Low Noise Terminal Operations," American Helicopter Society 53rd Annual Forum, Virginia Beach, VA, April-May 1997.
2. Edwards, B.D.: "XV-15 Low-Noise Terminal Area Operations Testing," NASA CR-1998-206946, February 1998.
3. Hardesty, M., Conner, D.A., Smith, C.D., Terrell, W.: "The Use of GPS Tracking and Guidance Systems for the Chicken Little Joint Project's 'Acoustic Week' Flight Test Program," American Helicopter Society 60th Forum, Baltimore, MD, May 7-10, 2004.
4. Spletstoeser, W.R., Kube, R., Seelhorst, U., Wagner, W., Boutier, A., Micheli, F., Mercker, E., Pengel, K.: "Higher Harmonic Control Aeroacoustic Rotor Test (HART) – Test Documentation and Representative Results," IB 129-95/28, Deutsche Forschungsanstalt für Luft- und Raumfahrt, December 1995.
5. van der Wall, B.G., Junker, B., Burley, C.L., Brooks, T.F., Yu, Y.H., Tung, C., Richard, H., Raffel, M., Wagner, W., Pengel, K., Mercker, E., Beaumier, P., Delrieux, Y.: "The HART II Test in the DNW – a Major Step towards Rotor Wake Understanding," 28th European Rotorcraft Forum, Bristol, UK, 2002.
6. Burley, C.L., Marcolini, M.A., Brooks, T.F., Brand, A.G., Conner, D.A.: "Tiltrotor Aeroacoustic Code (TRAC) Predictions and Comparison with Measurements," American Helicopter Society 52nd Annual Forum, Washington, D.C., June 4-6, 1996.
7. Burley, C.L., Brooks, T.F., Marcolini, M.A.: "Tiltrotor Aeroacoustic Code (TRAC) Assessment and Initial Comparison with TRAM Test Data," 25th European Rotorcraft Forum, Rome, Italy, September 1999.
8. Prichard, D.S., "Initial Tiltrotor Aeroacoustic Code (TRAC) Predictions for the XV-15 Flight Vehicle and Comparison with Flight Measurements," American Helicopter Society 56th Annual Forum, Virginia Beach, VA, May 2-4, 2000.
9. Boyd, Jr., D.D., Burley, C.L.: "Analysis of Measured and Predicted Acoustics from an XV-15 Flight Test," Helicopter Society 57th Annual Forum, Washington, D.C., May 9-11, 2001.
10. Upton, B., Ferrier, B.: "The Design, Development and Testing of the CL-227 Unmanned Air Vehicle (Sentinel and Sea Sentinel)," American Helicopter Society 51st Annual Forum, Fort Worth, TX, May 9-11, 1995.
11. Johnson, W.J.: "CAMRAD-II: Comprehensive Analytical Model for Rotorcraft Aerodynamics and Dynamics," Volumes 1-9, Johnson Aeronautics, Palo Alto, CA, 2004.
12. Brentner, K.S.: "Prediction of Helicopter Rotor Discrete Frequency Noise: A Computer Program Incorporating Realistic Blade Motions and Advanced Acoustic Formulation," NASA TM 87721, October 1986.
13. Brentner, K.S., Perez, G., Brès, G.A., Jones, H.E.: "Toward a Better Understanding of Maneuvering Rotorcraft Noise," American Helicopter Society 58th Annual Forum, Montréal, Canada, June 11-13, 2002.
14. Page, J.A., Plotkin, K.J., Downing, J.M.: "Rotorcraft Noise Model User's Guide," Wyle Research Report WR 00-20, August 2000.
15. Unidata: NetCDF (Network Common Data Form), <http://my.unidata.ucar.edu/content/software/netcdf/index.html>
16. Boyd, Jr., D.D., Burley, C.L., Conner, D.A.: "Full Scale Rotor Aeroacoustic Predictions and the Link to Model Rotor Data," American Helicopter Society 4th Decennial Specialists' Conference on Aeromechanics, San Francisco, CA, January 21-23, 2004.
17. Lim, J.W., Tung, C., Yu, Y.H., Burley, C.L., Brooks, T.F., Boyd, Jr., D.D., van der Wall, B., Schneider, O., Richard, H., Raffel, M., Beaumier, P., Bailey, J., Delrieux, Y., Pengel, K., Mercker, E.: "HART-II – Prediction of Blade Vortex Interaction Loading," 29th European Rotorcraft Forum, Friedrichshafen, Germany, September 16-18, 2003.
18. Johnson, W.J.: "Influence of Wake Models on Calculated Tilt Rotor Aerodynamics," American Helicopter Society Aerodynamics, Acoustics, and Test and Evaluation Specialists' Meeting, San Francisco, CA, January 23-25, 2002.
19. Page, J.A., Plotkin, K.J.: "Acoustic Repropagation Technique," Wyle Research Report WR 01-04, January 2001.
20. Coleman, C.P.: "A Survey of Theoretical and Experimental Coaxial Rotor Aerodynamics Research," NASA TP-3675, March 1997.